Electrochimica Acta 113 (2013) 575–582

Contents lists available at ScienceDirect

Electrochimica Acta

journal homepage: www.elsevier.com/locate/electacta

Mass-transfer characterization in a parallel-plate electrochemical reactor with convergent flow

A.N. Colli, J.M. Bisang*

Programa de Electroquímica Aplicada e Ingeniería Electroquímica (PRELINE), Facultad de Ingeniería Química, Universidad Nacional del Litoral, Santiago del Estero 2829, S3000AOM Santa Fe, Argentina

ARTICLE INFO

Article history:
Received 12 June 2013
Received in revised form 4 October 2013
Accepted 7 October 2013
Available online 14 October 2013

Keywords:
Convergent flow
Current distribution
Mass-transfer coefficient
Parallel-plate electrodes

ABSTRACT

A continuous reduction in the cross-section area is analysed as a means of improving mass-transfer in a parallel-plate electrochemical reactor. Experimental local mass-transfer coefficients along the electrode length are reported for different values of the convergent ratio and Reynolds numbers, using the reduction of ferricyanide as a test reaction. The Reynolds numbers evaluated at the reactor inlet range from 85 to 4600 with interelectrode gaps of 2 and 4 mm. The convergent flow improves the mean mass-transfer coefficient by 10–60% and mass-transfer distribution under laminar flow conditions becomes more uniform. The experimental data under laminar flow conditions are compared with theoretical calculations obtained by a computational fluid dynamics software and also with an analytical simplified model. A suitable agreement is observed between both theoretical treatments and with the experimental results. The pressure drop across the reactor is reported and compared with theoretical predictions.

1. Introduction

Reactors with parallel-plate electrodes are frequently used in applied electrochemistry. In many cases the reaction of interest is under mass-transfer control and several strategies are proposed to improve the reactor performance. One alternative is to place obstacles in the interelectrode gap to disturb hydrodynamics [1,2]. These are called turbulence promoters and mass-transfer conditions are strongly dependent on their geometric patterns [3]. The use of turbulence promoters makes the current distribution more uniform [3], but they increase the pressure drop along the reactor length [4] and can reduce the overall electrode surface area in the points where they make contact with the electrode [5]. They can also alter the residence time distribution in the reactor [6] and, depending on the turbulence promoter type, can produce the channelling of the electrolyte [7]. Another option is the increase of the roughness of the electrode [8], which enlarges the specific surface area and the mass-transfer coefficient, though Sedahmed and Shemilt [9] reported an insignificant influence under laminar flow conditions. A third alternative is the sparging of gas in the interelectrode gap or its generation at the electrode surface. In this last case the mass-transfer coefficient is increased owing to the disruption of the mass-transfer boundary layer, called bubble-induced convection [10]. This procedure increases the ohmic drop in the interelectrode gap [11] and modifies the current distribution at the electrode surface [12,13]. Mass-transfer due to bubble-induced convection was enhanced by the use of a rough electrode. However, when a turbulence promoter was placed in the flow channel, the influence upon the two-phase inert-gas mass-transfer was negligible [14]. Finally, another strategy to increase the efficiency of the equipment is changing its geometry. Thus, a sudden change in the flow cross-sectional area, as it may occur at the entrance and exit of electrochemical flow cells, produces important variations in the local mass-transfer coefficient [15]. Likewise, the use of corrugated ducts [16,17] increases the mass-transfer characteristics in relation to a smooth circular pipe. However, its implementation is difficult in the case of parallel-plate electrochemical reactors. Convergent and divergent ducts of rectangular cross-section were proposed to enhance heat transfer in the gas flow [18,19]. This paper is focused on this last alternative. Thus, the reduction in the cross-section inside the reactor is analysed in order to increase the flow velocity along the equipment to enlarge the mass-transfer coefficient. The main advantages of the proposal are the ease of construction and the fact that the electrode surface area is not modified in comparison when turbulence promoters are used.

2. Mathematical model

The stationary concentration of minority species in an electrochemical reactor with parallel-plate electrodes in the presence

* Corresponding author. Tel.: +54 342 4571164; fax: +54 342 4571164.
E-mail address: jbisang@fiq.unl.edu.ar (J.M. Bisang).

0013-4686/$ – see front matter © 2013 Elsevier Ltd. All rights reserved.
http://dx.doi.org/10.1016/j.electacta.2013.10.005

of supporting electrolyte is given by the convective mass-transfer equation as

$$D\left(\frac{\partial^2 c}{\partial x^2}+\frac{\partial^2 c}{\partial y^2}+\frac{\partial^2 c}{\partial z^2}\right)=u_x\frac{\partial c}{\partial x}+u_y\frac{\partial c}{\partial y}+u_z\frac{\partial c}{\partial z} \quad (1)$$

here x, y and z are the axial coordinates, c is the concentration of the reactant ion, D is the diffusion coefficient of the reactant in the solution, u_x, u_y and u_z are the velocities of fluid along the axial coordinates.

The numerical solution of the Navier–Stokes equations together with the continuity equation shows that, as demonstrated later, u_y for the present convergent reactor is negligible in comparison with the other components of the velocity vector. Then, assuming that

$$u_y = 0 \quad (2)$$

neglecting the change in concentration along the electrode width

$$\frac{\partial c}{\partial z}=0 \quad (3)$$

and

$$\frac{\partial^2 c}{\partial y^2}\gg\frac{\partial^2 c}{\partial x^2} \quad (4)$$

Eq. (1) is simplified to

$$D\frac{\partial^2 c}{\partial y^2}=u_x\frac{\partial c}{\partial x} \quad (5)$$

with the following boundary conditions [20]:

$$x=0,\quad c=c_{in}\quad \text{for}\quad 0<y<g \quad (6)$$

$$y=0,\quad c=c_s\quad \text{for}\quad x>0 \quad (7)$$

and a further condition is that the local concentration becomes uniform away from the vicinity of the electrode. Here c_{in} is the concentration at the reactor inlet, c_s at the electrode surface and g the interelectrode gap.

For a parallel-plate reactor with infinitely wide electrodes and fully developed laminar flow the Lévêque equation is [20]

$$u_x=\frac{12u_{av}}{d_h}y \quad (8)$$

here d_h is the hydraulic diameter and u_{av} is the average fluid velocity. Eq. (8) is supposed to be valid for convergent flow and, due to the small value of the interelectrode gap, d_h is not considered as a function of the position. Eq. (8) is a rough approximation, but it provides a very useful simplification for the modelling, which must be experimentally verified. Thus, the average fluid velocity in convergent flow is given by

$$u_{av}(x)=\frac{u_{av}(0)}{(1-\lambda x/L)} \quad (9)$$

where the convergence ratio, λ, is defined as

$$\lambda=1-\frac{W(L)}{W(0)} \quad (10)$$

here W is the electrode width.

Introducing Eqs. (8) and (9) into Eq. (5) results in

$$\frac{\partial^2 c}{\partial y^2}=\frac{12u_{av}(0)}{Dd_h(1-\lambda x/L)}y\frac{\partial c}{\partial x} \quad (11)$$

Likewise, the local mass-transfer coefficient, $k_{m,x}$ is given by

$$k_{m,x}=\frac{D}{(c_{in}-c_s)}\left.\frac{\partial c}{\partial y}\right|_{y=0} \quad (12)$$

Table 1
Values of the incomplete Beta functions and Ψ as a function of λ.

λ	$B_{\lambda/2}(2/3, 2/3)$	$B_{\lambda/2}(5/3, 2/3)$	Ψ
0.25	0.3816	0.0193	1.5680
0.50	0.6175	0.0631	1.6507
0.75	0.8269	0.1283	1.7547

Solving Eq. (11) with the boundary conditions given by Eqs. (6) and (7) and introducing the result into Eq. (12) yields

$$Sh_x=1.232\left[Re(0)Sc\frac{d_h}{x}\frac{1}{1-(\lambda x/2/L)}\right]^{1/3} \quad (13)$$

where the local Sherwood number, Sh_x, the Reynolds number evaluated at the reactor inlet, Re(0), and the Schmidt number, Sc, are defined as

$$Sh_x=\frac{k_{m,x}d_h}{D} \quad (14)$$

$$Re(0)=\frac{u_{av}(0)d_h}{\nu} \quad (15)$$

and

$$Sc=\frac{\nu}{D} \quad (16)$$

The mean Sherwood number, Sh, is given by

$$Sh=\frac{1}{A}\int_0^A Sh_x\,dA \quad (17)$$

here A is the active electrode surface area. Taking into account Eq. (10), Eq. (17) yields

$$Sh=\frac{1}{L(1-\lambda/2)}\int_0^L Sh_x(1-\lambda x/L)\,dx \quad (18)$$

Introducing Eq. (13) into Eq. (18) and solving results in

$$Sh=1.232\left[Re(0)Sc\frac{d_h}{L}\right]^{1/3}\Psi(\lambda) \quad (19)$$

being

$$\Psi(\lambda)=\frac{B_{\lambda/2}(2/3,2/3)-2B_{\lambda/2}(5/3,2/3)}{(1-\lambda/2)(\lambda/2)^{2/3}} \quad (20)$$

where $B_{\lambda/2}(2/3, 2/3)$ and $B_{\lambda/2}(5/3, 2/3)$ are the incomplete Beta function defined as

$$B_\omega(a,b)=\int_0^\omega t^{a-1}(1-t)^{b-1}\,dt \quad (21)$$

Table 1 reports $B_{\lambda/2}(2/3, 2/3)$, $B_{\lambda/2}(5/3, 2/3)$, and Ψ for different values of λ.

Likewise, for low values of λ Eq. (13) yields

$$\lim_{\lambda\to 0}Sh_x=1.232\left[Re(0)Sc\frac{d_h}{x}\right]^{1/3} \quad (22)$$

and from Eq. (19)

$$\lim_{\lambda\to 0}Sh=1.85\left[Re(0)Sc\frac{d_h}{L}\right]^{1/3} \quad (23)$$

Eqs. (22) and (23) were previously reported by Pickett [20] for a parallel-plate reactor with infinitely wide electrodes and developed laminar flow.

The OpenFOAM free software was also used to calculate the velocity and concentration fields. The velocity profiles inside the reactor were calculated, with the use of the simpleFoam routine, by solving numerically in laminar flow the Navier–Stokes equations

together with the continuity equation. The concentration field was computed with the use of the scalarTransportFoam routine via the velocity profiles previously obtained, both being in steady state. Introducing the slope of the concentration at the electrode surface in Eq. (12) the mass-transfer distribution was obtained along the electrode length. At the reactor inlet it was assumed that the profiles of concentration and velocity in the x direction are uniform, $u_y = u_z = 0$, and the gradient of pressure is zero. On the other hand, at the reactor outlet it was considered that the gradients of concentration and velocity are zero [21], whereas the pressure is zero. A non-slip boundary condition and gradients of pressure null were used at the solid walls. The concentration was set to zero at the working electrode and the concentration gradients were null for the other solid walls. The absolute tolerances for the calculation of velocity, pressure and concentration profiles were 1×10^{-5}, 1×10^{-6} and 1×10^{-6}, respectively. The relaxation factor was set to 0.3 for pressure and 0.7 for velocity according to the numerical scheme given in [22]. The computational region was divided into 160 by 85 by 75 structured elements in the x–y–z directions, respectively. A non-uniform mesh grading was used for the mesh size in the y direction, Δy, which was gradually varied according to a geometric progression with a ratio of 10 between the size of the last and the first cell. For the smallest cells, at the electrode surface, it was $\Delta y = 6 \times 10^{-6}$ m and 2×10^{-5} m for $d_h = 4$ mm and $d_h = 8$ mm, respectively. The quality of the discretization was tested by performing additional calculations for the case of a parallel-plate reactor with infinitely wide electrodes and developed laminar flow, where an analytical expression can be obtained for the local Sherwood number [20]. It was found that the numerical results, with 85 cells in the y direction, approach the analytical solution when the ratio of the geometric progression increases and the error between them becomes negligibly for a ratio of 10. The independence of the computed local Sherwood number on the grid size was checked.

3. Experimental

The determination of mass-transfer distribution was performed in an electrochemical reactor with parallel-plate electrodes employing a segmented cathode. The reactor was made of acrylic material with both electrodes of nickel, 100 mm wide and 250 mm long, arranged in a filter press configuration. The anode, a sheet of 1 mm thick, was electrically fed along its two lateral sides by means of copper current feeders, which were connected to the dc power supply at both ends to ensure isopotentiality of the metal phase. The cathode was made from 25 nickel segments, 100 mm wide, 9.5 mm high and 1 mm thick, which were insulated from one another by an epoxy resin of about 0.5 mm thick. The thickness of the insulating insertions between segments is in accordance with the recommendations given by Wein and Wichterle [23]. Calibrated resistors, 0.58 Ω resistance, were inserted between the backside of each segment and the cathodic current feeder, which was electrically connected at both ends. By measuring the ohmic drop in the resistors, it was possible to determine the axial current distribution and to calculate the mass-transfer coefficient at each segment, $k_{m,s}$, according to:

$$k_{m,s} = \frac{I_{lim}}{\nu_e F W l c_{in}} \tag{24}$$

which approaches the local value, $k_{m,x}$. Here I_{lim} is the limiting current at each segment, l is the segment length, W is the segment active width, ν_e is the number of electrons interchanged and F is the Faraday constant. The use of a segmented electrode allows to calculate the mean mass-transfer coefficient at each segment, which approaches the local value when smaller is the size of the segment. However, in our previous paper [3], it was concluded that the size of the segments is appropriate to determine local mass-transfer coefficients. Data acquisition was performed simultaneously in all segments using a computer controlled, home made analogue multiplexer.

The lower and upper parts of the reactor present chambers of a triangular cross-sectional area, with perpendicular nozzles for the inlet and outlet of the electrolyte. The convergent flow inside the reactor was achieved by using gaskets of the appropriate shape as it is shown in Fig. 1 in order to obtain convergence ratios of 0.25, 0.5 and 0.75. Two interelectrode gaps were used, 2.0 and 4.0 mm, which were fixed by the thickness of the gasket.

The test reaction was the electrochemical reduction of ferricyanide from solutions with $[K_3Fe(CN)_6] \cong 0.01$ mol dm^{-3}, $[K_4Fe(CN)_6] \cong 0.01$ mol dm^{-3}, in 0.65 mol dm^{-3} of K_2CO_3 as supporting electrolyte, while the reverse reaction occurred at the anode. Table 2 summarizes the composition and physicochemical properties of the solution. Samples of the solution were taken from the reservoir after each experiment and the ferricyanide concentration was spectrophotometrically determined. Nitrogen was bubbled in the reservoir for 1 h prior to the experiment in order

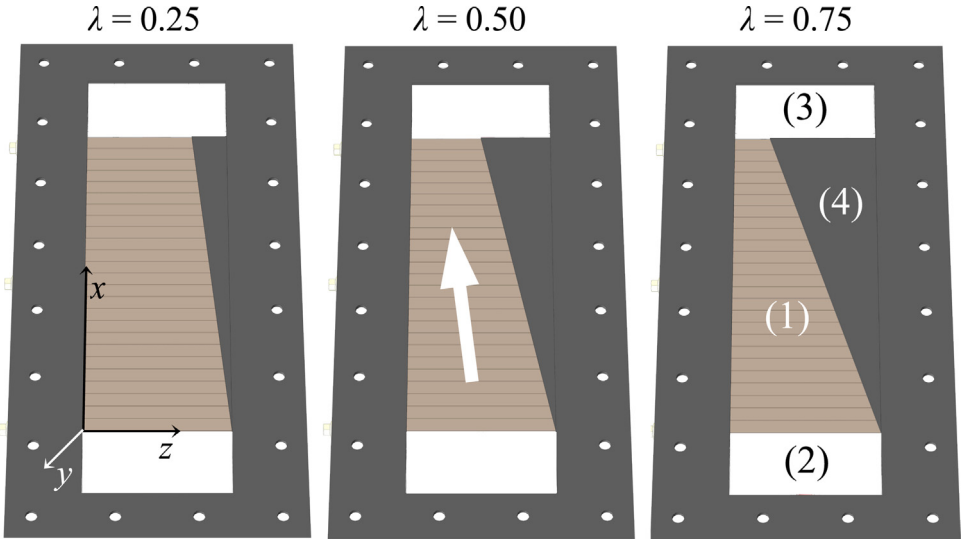

Fig. 1. Schematic views of the segmented cathode showing the geometric shape of the gasket to produce a convergent flow. (1) Segmented cathode; (2) electrolyte inlet; (3) electrolyte outlet; and (4) gasket.

Table 2
Properties of the electrolyte.

Composition	$[K_3Fe(CN)_6] = 0.01$ M $[K_4Fe(CN)_6] = 0.01$ M $[K_2CO_3] = 0.65$ M
Kinematic viscosity (m^2/s)	1.31×10^{-6}
Diffusion coefficient (m^2/s)	8.10×10^{-10}
Sc	1617
ν_e	1

to remove the dissolved oxygen. The experiments were carried out potentiostatically at −0.3 V, the cathodic potential was controlled against a saturated calomel electrode connected to a Haber–Luggin capillary positioned in the middle region of the cathode. However, the cathodic potential was also measured near the reactor entrance and at the reactor exit in order to ensure that all the segments in the cathode were under limiting current conditions. These ports were also used in additional experiments to measure the pressure drop across the reactor with a manometer using carbon tetrachloride as manometric liquid. The reactor was made part of a flow circuit system consisting of a pump, a flow metre, a reservoir and connections to maintain the temperature at the preset value, 30 °C.

Further details of the equipment employed, method of operation, data acquisition, test reaction and reagents can be obtained from our previous work [24].

4. Results and discussion

Fig. 2 shows typical curves of the local mass-transfer coefficient as a function of the axial position for different values of the convergence ratio and Reynolds numbers. The full line represents the theoretical behaviour for a parallel-plate electrochemical reactor with infinitely wide electrodes and fully developed laminar flow, Eq. (22). It can be observed that, depending on the Reynolds number, the increase in λ modifies the local mass-transfer coefficient mainly in the region near the reactor outlet. Thus, a change in λ produces two effects on the mass-transfer performance: (i) to alter the uniformity of the mass-transfer behaviour and (ii) to modify the mean mass-transfer coefficient. To analyse the uniformity of the distribution, Fig. 3 reports the mean relative deviation, δ_{mean}, of the experimental data, calculated as

$$\delta_{mean} = \frac{1}{N}\sum_{1}^{N}\left|\frac{k_{m,x}}{k_{m,mean}} - 1\right| \quad (25)$$

where $k_{m,mean}$ is the mean value of the mass-transfer coefficient and N is the number of experimental points, 25. The distribution of the local mass-transfer coefficient is more uniform as δ_{mean} is smaller. It is reported as a full line the theoretical mean relative deviation for a parallel-plate electrochemical reactor with infinitely wide electrodes and fully developed laminar flow, $(2/3)^3$. Fig. 3 shows two well different regions, the first is at Reynolds numbers lower than 500 where all the points in the reactor are under laminar flow conditions independent of the λ value. In this region, the behaviour for λ = 0 is close to the theoretical prediction and when λ increases the mass-transfer distribution becomes more uniform, lower δ_{mean}. This effect is more pronounced for the high value of the interelectrode gap. The second region is detected at Reynolds numbers higher than 3000 where all the points along the reactor are in turbulent flow conditions. In this region no improvement of the uniformity of the mass-transfer coefficient is observed with the use of a convergent duct. Then, considering the mass-transfer uniformity the use of a convergent duct is only interesting under

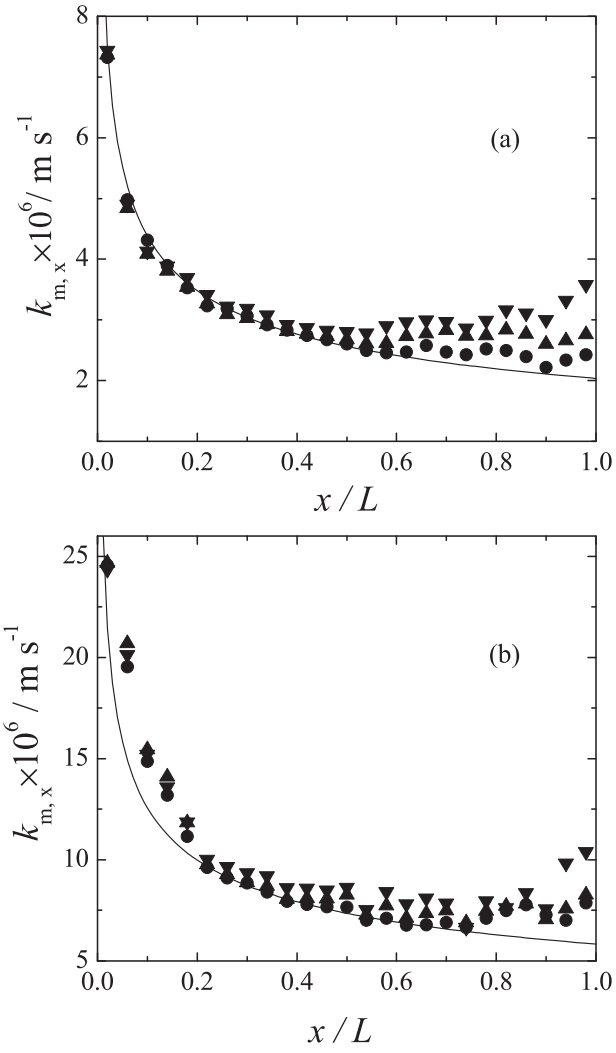

Fig. 2. Experimental local mass-transfer coefficient as a function of the axial position for different λ values and Reynolds numbers evaluated at the reactor inlet. Part (a): d_h = 8 mm, Re(0) = 84. Part (b): d_h = 4 mm, Re(0) = 496. (●): λ = 0.25. (▲): λ = 0.50. (▼): λ = 0.75. Full line: theoretical behaviour according to Eq. (22).

laminar flow conditions. Fig. 4 reports the uniformity factor defined as

$$UF = 1 - \frac{\delta_{mean}(\lambda)}{\delta_{mean}(\lambda = 0)} \quad (26)$$

According to Eq. (26) the uniformity factor ranges from 0, no uniform distribution, to 1 when the mass-transfer distribution is totally uniform. Fig. 4 shows that more uniform mass-transfer distributions under laminar flow conditions are achieved at low Reynolds numbers, high λ and high interelectrode gaps.

Fig. 5 reports the effect of both the Reynolds number and λ on the mass-transfer enhancement factor calculated as

$$EF = \frac{k_{m,mean}(\lambda)}{k_{m,mean}(\lambda = 0)} \quad (27)$$

It is observed that the mass-transfer enhancement factor always increases with the Reynolds number. Likewise, this factor is enlarged when the flow is constricted, which is more pronounced under turbulent flow conditions. Moreover, the increase in the interelectrode gap diminishes the enhancement factor and this effect is remarked in the case of turbulent flow. From the experimental data reported in Figs. 3 and 5 it can be concluded that under turbulent flow conditions a convergent duct is unimportant in order to obtain uniformity in the local mass-transfer coefficient

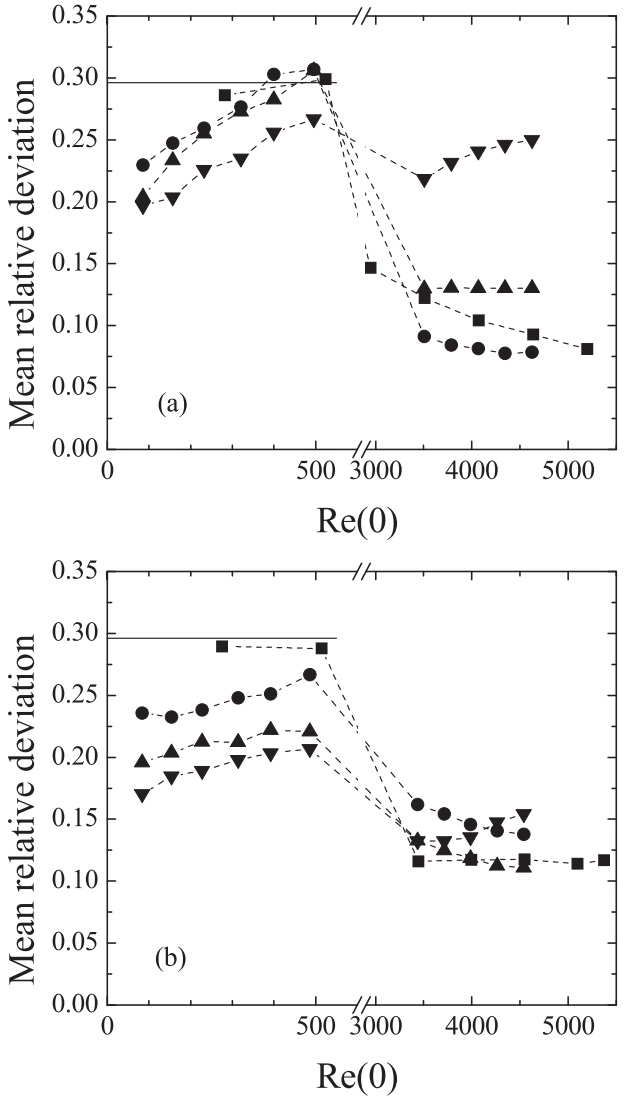

Fig. 3. Mean relative deviation for mass-transfer distribution as a function of the Reynolds number evaluated at the reactor inlet for different λ values. Part (a): d_h = 4 mm. Part (b): d_h = 8 mm. (■): λ = 0. (●): λ = 0.25. (▲): λ = 0.50. (▼): λ = 0.75. Full line: theoretical mean relative deviation for λ = 0.

and considering the enhancement of mass-transfer conditions a better performance can be achieved with the use of turbulence promoters [3]. For this reason the following discussion and comparison of experimental and theoretical results will be focussed on laminar flow conditions.

Fig. 6 shows, according to computational fluid dynamics calculations, the velocity profiles at small distances from the electrode surface in the *y* direction in three points along the electrode length. The modulus of the velocity vector is also reported. Similar results were obtained for other *z* values along the electrode width. It can be observed that the velocity component in the *y* coordinate is near zero in all points, which confirms Eq. (2) and u_x overlaps the modulus of the velocity vector. Thus, to satisfy the continuity equation the changes of u_x with the position are mainly counteracted by the variation of u_z.

The numerical calculations do not show any important differences of the local Sherwood number along the electrode width, corroborating Eq. (3). As expected, changes are only observed at the edges of the electrode as it is reported in Fig. 7.

Fig. 8 reports the theoretical local Sherwood number as a function of the axial position in the reactor for different values of

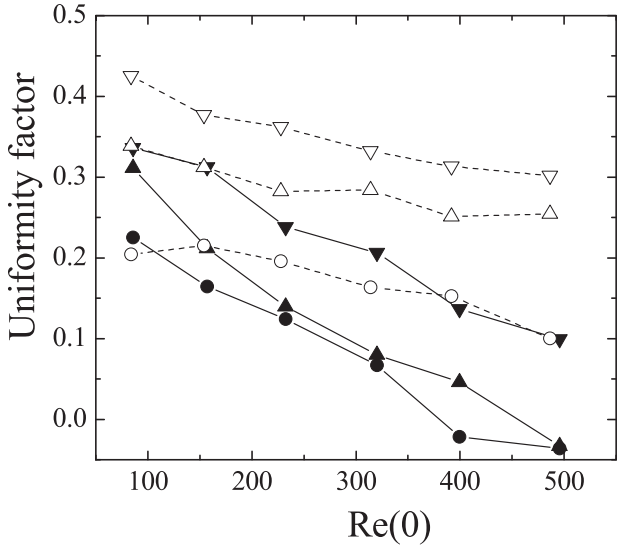

Fig. 4. Uniformity factor for mass-transfer distribution as a function of the Reynolds number evaluated at the reactor inlet for different λ values. Full symbols: d_h = 4 mm. Open symbols: d_h = 8 mm. (●) and (○): λ = 0.25. (▲) and (△): λ = 0.50. (▼) and (▽): λ = 0.75.

the convergence ratio, the hydraulic diameter and the Reynolds number. The symbols were obtained from calculations using computational fluid dynamics and the lines correspond to Eq. (13). A close agreement is observed between the numerical results and those from Eq. (13). However, a small discrepancy between them is detected at the reactor outlet for high values of convergence ratio. This effect is more pronounced when the hydraulic diameter is increased. Moreover, the numerical results show a minimum in the mass-transfer distribution at high values of the convergence ratio, which is not predicted by Eq. (13), and it is a consequence of a change in the velocity profile at the reactor outlet. From Fig. 8, it can be concluded that in comparison with the numerical procedure, the simplified model represented by Eq. (13) yields suitable results. The inset in Fig. 8 shows the ratio between the theoretical local Sherwood number and its mean value as a function of the axial position according to computational fluid dynamics calculations. Fig. 8 confirms the experimental conclusion that the increase

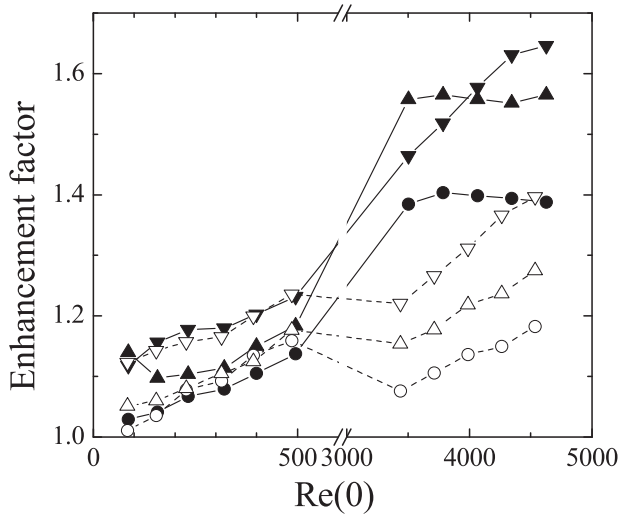

Fig. 5. Mass-transfer enhancement factor as a function of the Reynolds number evaluated at the reactor inlet for different λ values. Full symbols: d_h = 4 mm. Open symbols: d_h = 8 mm. (●) and (○): λ = 0.25. (▲) and (△): λ = 0.50. (▼) and (▽): λ = 0.75.

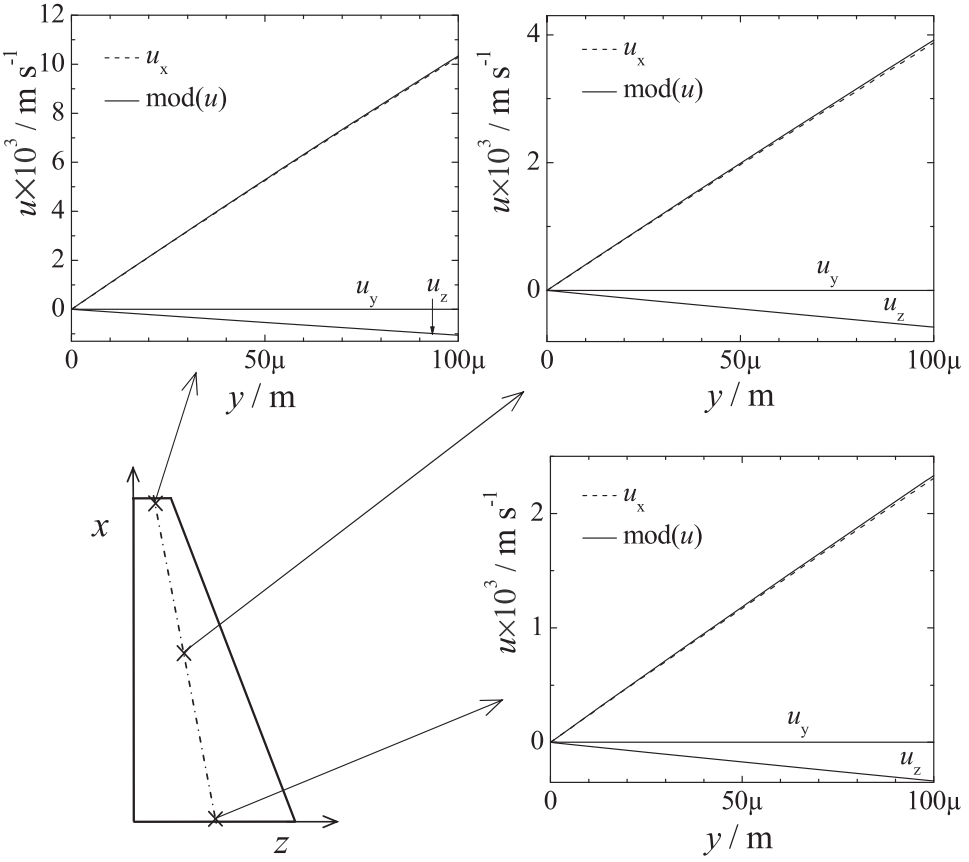

Fig. 6. Modulus of velocity vector and velocity profiles for u_x, u_y and u_z in the y direction at three points along the electrode length calculated by computational fluid dynamics. d_h = 8 mm. λ = 0.75. $W(0)$ = 0.1 m. L = 0.25 m. Re(0) = 92.

in the convergence ratio makes mass-transfer distribution more uniform.

In Fig. 9 the distributions of the local Sherwood number for typical experiments performed at different Reynolds numbers and convergence ratios are compared with theoretical results obtained from Eq. (13). The theoretical predictions agree well with the experimental results and the discrepancy between them is higher at the reactor outlet when the convergence ratio is increased. Moreover, the experimental results also show a minimum of the mass-transfer coefficient in the vicinity of the reactor outlet, which was also observed in the data obtained by computational fluid dynamics

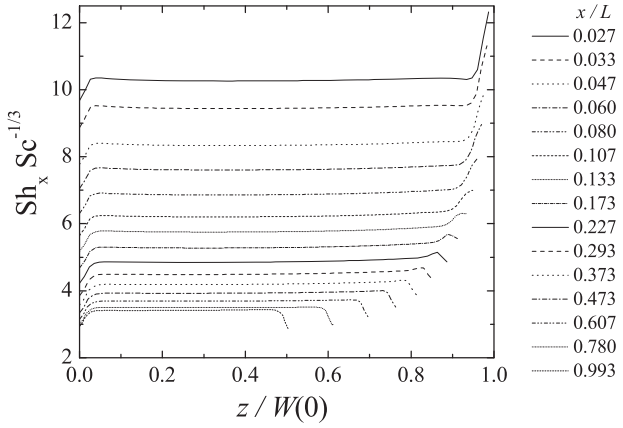

Fig. 7. Local Sherwood number along the electrode width at different axial positions according to computational fluid dynamics calculations. d_h = 8 mm. λ = 0.50. Re(0) = 403.

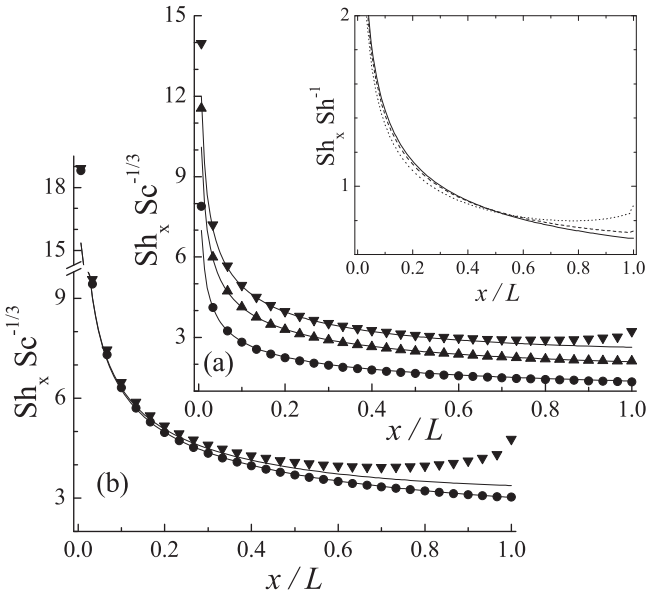

Fig. 8. Comparison of the theoretical values of the local Sherwood number as a function of the axial position in the reactor for different values of the convergence ratio and the Reynolds number. Symbols: theoretical behaviour according to computational fluid dynamics. Lines: Eq. (13). Part (a): d_h = 4 mm. (●): λ = 0.25, Re(0) = 76. (▲): λ = 0.50, Re(0) = 229. (▼): λ = 0.75, Re(0) = 382. Part (b): d_h = 8 mm. (●): λ = 0.25, Re(0) = 403. (▼): λ = 0.75, Re(0) = 403. Inset: Ratio between the local Sherwood number to its mean value according to computational fluid dynamics calculations. d_h = 4 mm. Re(0) = 382. Full line: λ = 0.25. Dashed line: λ = 0.50. Dotted line: λ = 0.75.

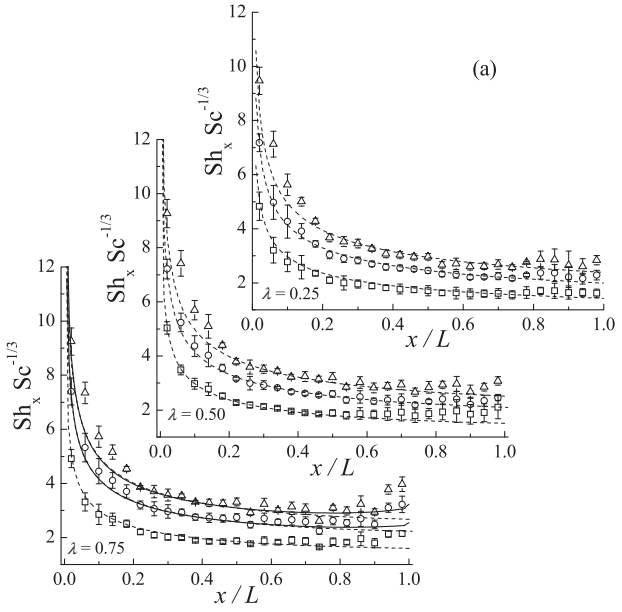

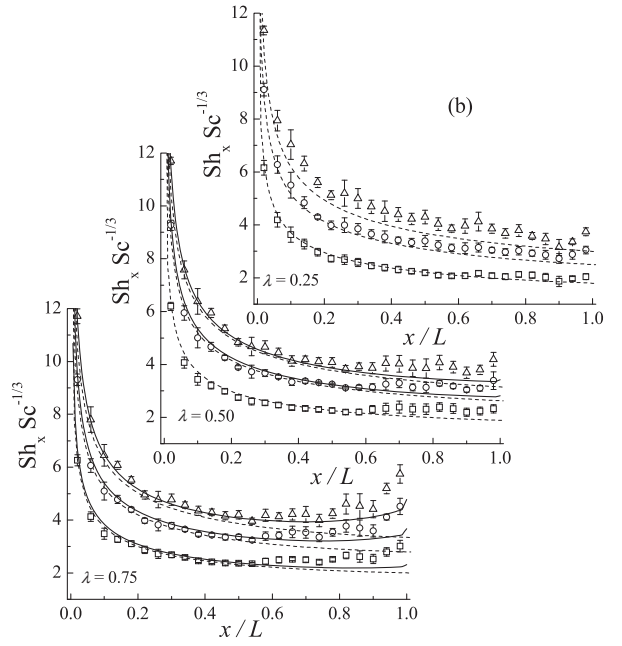

Fig. 9. Local Sherwood number as a function of the axial position in the reactor for different values of the Reynolds number and the convergence ratio. Part (a): d_h = 4 mm. (□): Re(0) = 86. (○): Re(0) = 232. (△): Re(0) = 399. Part (b): d_h = 8 mm. (□): Re(0) = 84. (○): Re(0) = 228. (△): Re(0) = 392. Vertical segments: standard deviation. Full lines: computational fluid dynamics calculations. Dashed lines: theoretical behaviour according to Eq. (13).

calculations reported as full lines. However, this minimum is little pronounced and it does not present a significant influence on the mass-transfer performance of the electrochemical reactor. In all the other cases a full overlapping between both theoretical results was observed.

Fig. 10 compares the local mass-transfer results with the behaviour given by Eq. (13). In this figure 900 points are represented, which correspond to all the experimental results obtained for different values of the convergence ratio, the Reynolds number and the hydraulic diameter. It can be observed a satisfactory agreement of the experimental data with the theoretical prediction given by Eq. (13). The points showing the higher discrepancy with

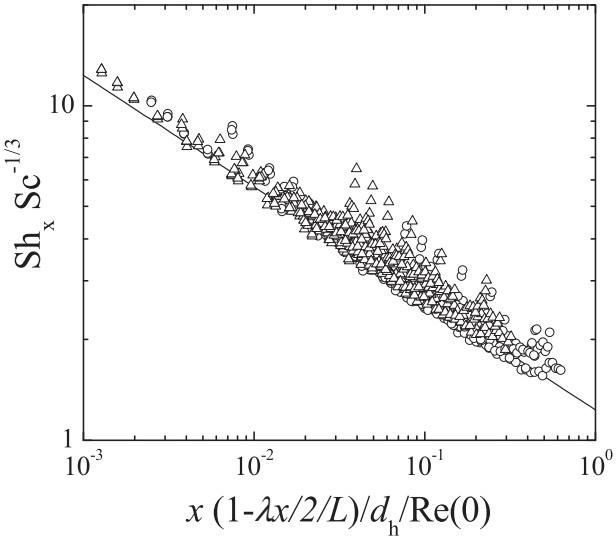

Fig. 10. Comparison of the local mass-transfer results with the theoretical model. Full line: Eq. (13). Symbols: experimental points. (○): d_h = 4 mm. (△): d_h = 8 mm.

the theoretical model were measured at the reactor outlet with the higher value of the convergence ratio.

Fig. 11 shows the mean values of the Sherwood number as a function of a dimensionless abscissa. The symbols (★) were obtained by computational fluid dynamics calculations and the full line corresponds to Eq. (19). A close agreement is observed between both theoretical treatments and also with experimental data.

The pressure drop across the reactor, ΔP, was obtained from

$$\Delta P = \Delta P_{\mathrm{mes}} - 0.5\rho[u_{\mathrm{av}}^2(L) - u_{\mathrm{av}}^2(0)] \tag{28}$$

where ΔP_{mes} was the pressure difference shown on the manometer and the friction factor, f, was calculated as

$$f = \frac{\Delta P}{4L} \times \frac{[d_h(0) + d_h(L)]/2}{\rho/2\left\{[u_{\mathrm{av}}(0) + u_{\mathrm{av}}(L)]/2\right\}^2} \tag{29}$$

being ρ the density. Fig. 12 shows the friction factor as a function of the mean Reynolds number, $\mathrm{Re}_{\mathrm{mean}}$, calculated with the

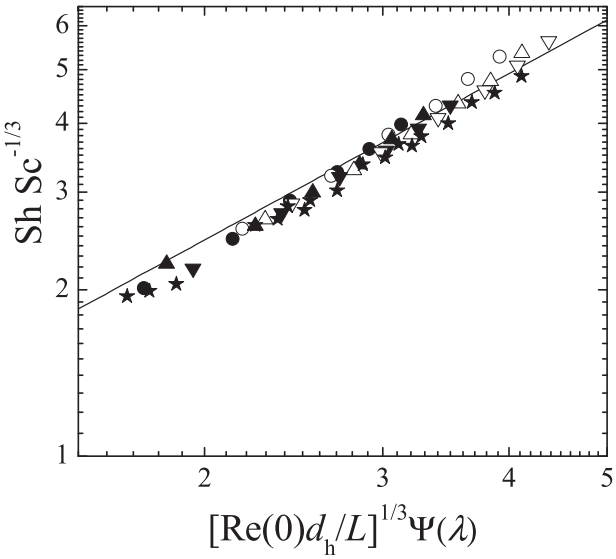

Fig. 11. Comparison of the experimental and theoretical mean Sherwood numbers. Full symbols: d_h = 4 mm. Open symbols: d_h = 8 mm. (●) and (○): λ = 0.25. (▲) and (△): λ = 0.50. (▼) and (▽): λ = 0.75. (★): Theoretical behaviour according to computational fluid dynamics. Full line: Eq. (19).

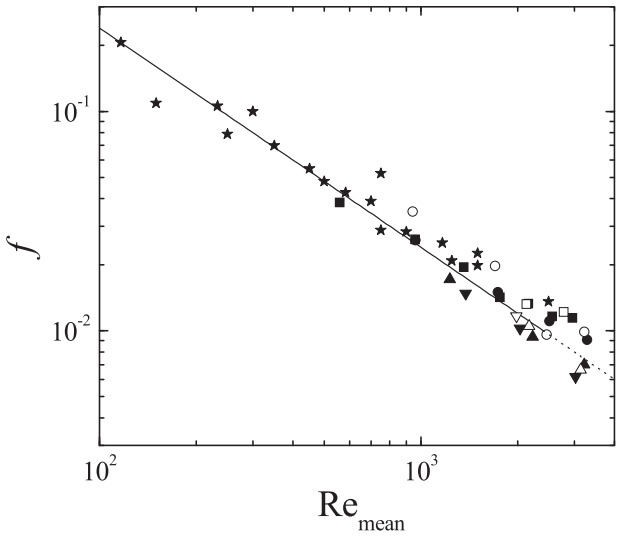

Fig. 12. Friction factor as a function of the Reynolds number calculated with mean values of the fluid velocity and hydraulic diameter. Full symbols: interelectrode gap = 2 mm. Open symbols: interelectrode gap = 4 mm. (■) and (□): λ = 0. (●) and (○): λ = 0.25. (▲) and (△): λ = 0.50. (▼) and (▽): λ = 0.75. (⋆): Theoretical behaviour according to computational fluid dynamics. Full line: Eq. (30).

mean values of the fluid velocity and the hydraulic diameter, which explains the scattering of the results. The symbols (⋆) were obtained by computational fluid dynamics calculations and the full line represents the following theoretical equation [25]:

$$f = \frac{24}{Re_{mean}} \tag{30}$$

A close agreement is observed between the experimental pressure drops with both theoretical models.

5. Conclusions

- Under laminar flow conditions, the use of a convergent duct enhances the mass-transfer rate by 5–20% and also its distribution becomes more uniform along the electrode length. Both effects are increased when the convergence ratio is enlarged.
- Under turbulent flow conditions, the use of a convergent duct improves the mass-transfer by 10–60%, being this strongly dependent on the interelectrode gap. However, a poor effect was detected on the uniformity factor.
- The experimental results under laminar flow conditions can be properly predicted by computational fluid dynamics calculations.
- A simplified mathematical model was developed, which shows a suitable agreement with the experimental results. Small discrepancies were observed at the reactor outlet at high values of the convergence ratio.
- A similar behaviour to predict the mean mass-transfer coefficient was observed for both theoretical models with a good agreement with the experimental results.
- The experimental pressure drop across the reactor shows a close agreement with the theoretical prediction.
- The use of a convergent duct of rectangular cross-section for the interelectrode gap enhances the mass-transfer performance of electrochemical reactors without introducing difficulties in the constructive features of the equipment. Moreover, this concept is directly applicable to existing parallel-plate reactors by changing the shape of the gaskets.

Acknowledgements

This work was supported by the Agencia Nacional de Promoción Científica y Tecnológica (ANPCyT), Consejo Nacional de Investigaciones Científicas y Técnicas (CONICET) and Universidad Nacional del Litoral (UNL) of Argentina.

References

[1] D. Pletcher, F.C. Walsh, Industrial Electrochemistry, Chapman and Hall, London, 1993, pp. 344 (Chapter 7).
[2] F. Cœuret, A. Storck, Elements de Genie Electrochimique, TEC&DOC, Paris, 1984, pp. 148 (Chapter 3b).
[3] A.N. Colli, R. Toelzer, M.E.H. Bergmann, J.M. Bisang, Mass-transfer studies in an electrochemical reactor with a small interelectrode gap, Electrochimica Acta 100 (2013) 78.
[4] M. Griffiths, C. Ponce de León, F.C. Walsh, Mass transport in the rectangular channel of a filter-press electrolyzer (the FM01-LC reactor), AIChE Journal 51 (2005) 682.
[5] M. Venkatraman, J. Van Zee, Effect of a net on the limiting current distribution in a parallel plate electrochemical reactor: part I. Individual effects, Journal of Applied Electrochemistry 39 (2009) 1425.
[6] Á. Frías-Ferrer, J. González-García, V. Sáez, C. Ponce de León, F.C. Walsh, The effects of manifold flow on mass transport in electrochemical filter-press reactors, AIChE Journal 54 (2008) 811.
[7] A.N. Colli, J.M. Bisang, Evaluation of the hydrodynamic behaviour of turbulence promoters in parallel plate electrochemical reactors by means of the dispersion model, Electrochimica Acta 56 (2011) 7312.
[8] I. Roušar, V. Cezner, Mass transfer coefficients and friction coefficients for rough electrodes, Institution of Chemical Engineers Symposium Series 98 (1986) 85.
[9] G.H. Sedahmed, L.W. Shemilt, Forced convection mass transfer at rough surfaces in annuli, Letters in Heat and Mass Transfer 3 (1976) 499.
[10] A. Shah, J. Jorne, Mass transfer under combined gas evolution and forced convection, Journal of the Electrochemical Society 136 (1989) 153.
[11] F. Hine, K. Murakami, Bubble effects on the solution IR drop in a vertical electrolyzer under free and forced convection, Journal of the Electrochemical Society 127 (1980) 292.
[12] H.F.M. Gijsbers, L.J.J. Janssen, Distribution of mass transfer over a 0.5-m-tall hydrogen-evolving electrode, Journal of Applied Electrochemistry 19 (1989) 637.
[13] J.M. Bisang, Effect of mass transfer on the current distribution in monopolar and bipolar electrochemical reactors with a gas-evolving electrode, Journal of Applied Electrochemistry 23 (1993) 966.
[14] D.J. Economou, R.C. Alkire, Two-phase mass transfer in channel electrolyzers with gas–liquid flow, Journal of Electrochemical Society 132 (1985) 601.
[15] A.A. Wragg, D.J. Tagg, M.A. Patrick, Diffusion-controlled current distributions near cell entries and corners, Journal of Applied Electrochemistry 10 (1980) 43.
[16] M. Gradeck, M. Lebouché, Wall shear measurements inside corrugated channels using the electrochemical technique, Experiments in Fluids 24 (1998) 17.
[17] S.D. Hwang, I.H. Jang, H.H. Cho, Experimental study on flow and local heat/mass transfer characteristics inside corrugated duct, International Journal of Heat and Fluid Flow 27 (2006) 21.
[18] C.-C. Su, H. Lin, Heat transfer and pressure drop characteristics of flow in convergent and divergent ducts, International Journal of Energy Research 15 (1991) 581.
[19] C.-C. Su, R.-H. Lin, Experimental studies on flow in convergent and divergent ducts of rectangular cross section, International Journal of Energy Research 21 (1997) 77.
[20] D.J. Pickett, Electrochemical Reactor Design, 2nd ed., Elsevier, Amsterdam, 1979 (Chapter 4).
[21] H.H.K. Versteeg, W. Malalasekera, An Introduction to Computational Fluid Dynamics: The Finite Volume Method, Prentice Hall, London, 2007 (Chapter 9).
[22] User Guide of OpenFOAM, http://www.openfoam.org/docs/user/
[23] O. Wein, K. Wichterle, Theory of segmented electrodifussion probes: the effect of insulating insertions, Collection of Czechoslovak Chemical Communication 54 (1989) 3198.
[24] A.N. Colli, J.M. Bisang, Validation of theory with experiments for local mass transfer at parallel plate electrodes under laminar flow conditions, Journal of the Electrochemical Society 160 (2013) E5.
[25] F.M. White, Fluid Mechanics, 4th ed., McGraw Hill, Boston, 1998, pp. 359 (Chapter 6).